Doping effect on magnetic and transport properties of $Pr_{2-x}Sr_xCoO_4$

2008 J. Phys.: Condens. Matter 20 395213

(http://iopscience.iop.org/0953-8984/20/39/395213)

J. Phys.: Condens. Matter **20** (2008) 395213 (9pp) doi:10.1088/0953-8984/20/39/395213

Doping effect on magnetic and transport properties of $Pr_{2-x}Sr_xCoO_4$

S L Huang[1], Z C Fan[1], J B Yi[2], B C Zhao[1], Y Wu[1], K Q Ruan[3], M Li[3], J Ding[2] and L Wang[1]

[1] Division of Physics and Applied Physics, School of Physical and Mathematical Science, Nanyang Technological University, Singapore 637371, Singapore
[2] Department of Material Science and Engineering, National University of Singapore, Singapore 117576, Singapore
[3] Department of Physics, University of Science and Technology of China, Hefei, Anhui 230026, People's Republic of China

E-mail: kqruan@ustc.edu.cn and WangLan@ntu.edu.sg

Received 23 February 2008, in final form 15 August 2008
Published 1 September 2008
Online at stacks.iop.org/JPhysCM/20/395213

Abstract

We present the results of a systematic investigation of the dc magnetization, ac susceptibility, resistivity and thermopower of $Pr_{2-x}Sr_xCoO_4$ ($x = 1.2$, 1.3 and 1.5). The $x = 1.2$ specimen undergoes a paramagnetic phase above 201.57 K, Griffiths phase between 201.57 and 129.24 K, ferromagnetic cluster-glass phase between 129.24 and 16.19 K and spin-glass state reentrance below 16.19 K. With increasing Sr content, the Griffiths phase and the spin-glass state are suppressed. The specimen shows a p-type semiconducting conduction changing from thermally activated conduction to variable range hopping conduction with increasing Sr doping level. The rich magnetic and transport behaviors are suggested due to the complicated magnetic interactions and Jahn–Teller distortion of the cobalt ions associated with small polarons.

1. Introduction

Cobalt oxides with perovskite structure have attracted much attention due to the subtle balance between the crystal field splitting Δ and the intersite interaction energy (Hund's rule coupling) J of the Co^{3+} ion in the octahedral coordination, in addition to a small energy difference between the low-spin (LS, t_{2g}^6) state, intermediate-spin (IS, $t_{2g}^5e_g^1$) state and high-spin (HS, $t_{2g}^4e_g^2$) state. Much effort has been devoted to the three-dimensional (3D) perovskite oxides $Ln_{1-x}Sr_xCoO_3$ (Ln = La, rare-earth elements) [1–5]. The $LaCoO_3$ is a diamagnetic insulator based on the LS Co^{3+} ground state and undergoes a transition to a paramagnetic state around 100 K due to thermal population of IS and/or HS states. The hole doping affects the spin state of Co^{3+} in a similar way to temperature. The system undergoes a crossover from spin/cluster-glass semiconductor to ferromagnetic metal upon doping, but the substitution of the nonmagnetic ion La^{3+} by the magnetic ion Nd^{3+} induces antiferromagnetic order between the Nd and Co sublattices.

$Ln_{2-x}Sr_xCoO_4$, another cobalt oxide system with layered perovskite structure, has been the subject of a small number of investigations, most of which have focused on the system with nonmagnetic rare-earth elements, Ln = La and Y [6–11]. The La_2CoO_4 is an antiferromagnetic insulator with an HS state of Co^{2+} ions. The Sr doping brings the Co^{3+} ions and a spin-state transition of Co^{3+} ions from the HS state to IS state in $x < 1.0$, and the system with $x = 0.5$ exhibits a checkerboard pattern of charge ordering below 800 K. At high doping ($x > 1.0$) the system presents abundant magnetic features at various temperatures. It shows a paramagnetic phase, Griffiths phase, ferromagnetic phase and spin-glass state reentrance with decreasing temperature from 300 to 4.2 K. The result is similar to the recent research on $Nd_{2-x}Sr_xCoO_4$ [12], but is very different from the parent compound Sr_2CoO_4 [13] and the series $Y_{2-x}Sr_xCoO_4$ [11]. Both of them go through a paramagnetic phase to a ferromagnetic phase as the temperature decreases. In fact, the presence of rock-salt layer LnO disturbs the 3D periodicity of the perovskite structure, and the two-dimensional (2D) confinement of the Co–O–Co network significantly reduces the bandwidth of the e_g electrons in the system. Doping with different size and magnetic/nonmagnetic rare-earth ions would induce more complex and intriguing physical properties. It has been reported that the single-layered perovskite cobaltite $PrSrCoO_4$

exhibits a semiconducting-paramagnetic behavior without any spin/cluster-glass phase [14]. To further study the doping effect on the Sr_2CoO_4-based layered structure cobaltite, we carried out systematic experiments on the magnetic and transport properties of $Pr_{2-x}Sr_xCoO_4$ with $x = 1.2$, 1.3 and 1.5.

2. Experimental considerations

Polycrystalline specimens $Pr_{2-x}Sr_xCoO_4$ ($x = 1.2$, 1.3 and 1.5) were prepared by the nitrate decomposition method [15]. Preliminary compounds for the reaction are Pr_6O_{11} (99.9%), $SrCO_3$ (99.9+%), $Co(NO_3)_2{\cdot}6H_2O$ (99.999%) and KNO_3 (99.0%) powder. Firstly, a stoichiometric mixture of Pr_6O_{11}, $SrCO_3$ and $Co(NO_3)_2{\cdot}6H_2O$ was initially dissolved in HNO_3 (65%) and gently warmed up to evaporate the solvent. The resulting mixture of nitrates was mixed with KNO_3 powder in a molar ratio of $1Co(NO_3)_2{\cdot}6H_2O{:}1KNO_3$, which was subsequently heated at 450 °C for 1 h followed by a treatment at 650 °C for 48 h. The reacted powder was then thoroughly ground and calcined in air three times at 850–950 °C for 24 h. After regrinding, the sample was pressed into pellets and finally annealed in air at 975 °C for 24 h. The phase structure of the specimens was examined by powder x-ray diffraction (XRD) with a Bruker AXS D8 advanced powder diffractometer using Cu Kα radiation. DC magnetic measurement and electric transport measurement were performed with corresponding options, including the vibration sample magnetometer and ac electric transport in a physical property measurement system (Quantum Design). The dc magnetization measurements, including magnetic hysteresis loop and magnetization versus temperature with zero-field-cooling (ZFC) and field-cooling (FC) processes, were made in the temperature range 5 K $\leqslant T \leqslant$ 300 K with a magnetic field up to 50 kOe. AC susceptibility was measured in a superconducting quantum interference device (Magnetic Property Measurement System, Quantum Design) in the frequency range 1 Hz $\leqslant f \leqslant$ 1 kHz. Electric conductivity was measured from 10 to 310 K. Thermopower was measured in the temperature range 20 K $\leqslant T \leqslant$ 300 K on home-built apparatus as described in [12].

3. Results and discussion

Figure 1 shows the powder XRD patterns of $Pr_{2-x}Sr_xCoO_4$ ($x = 1.2$, 1.3 and 1.5) at room temperature. All the observed diffraction peaks can be indexed based on the tetragonal structure with space group $I4/mmm$ similar to that of the undoped Sr_2CoO_4 system [11]. All the specimens are a single phase with no detectable secondary phases.

Temperature dependence of the ZFC and FC magnetizations and inverse dc susceptibilities for $Pr_{2-x}Sr_xCoO_4$ is shown in figure 2. The FC and ZFC data were measured in a warming-up procedure with an applied field of 1 kOe after field cooling (1 kOe) and zero-field cooling from 300 K, respectively. To eliminate the influence of the residual magnetization in the measuring system, the magnetic field was decreased to zero from 20 kOe in an oscillation model before the measurement. The ZFC $M(T)$ of all three samples exhibits a sharp peak around a temperature, T_{CG}, which can be interpreted in terms of

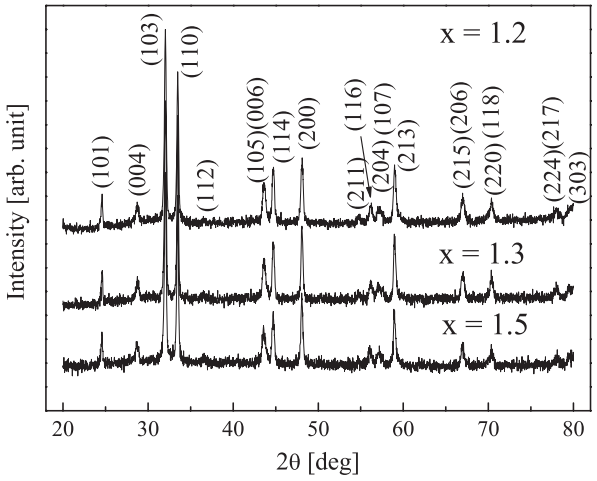

Figure 1. Powder x-ray diffraction patterns of $Pr_{2-x}Sr_xCoO_4$ at room temperature.

the ferromagnetic cluster model. It is postulated that the chemically single-phase cobaltite is not magnetically homogeneous. The magnetic phase of the system separates into ferromagnetic clusters and an antiferromagnetic matrix. The existence of a peak in the ZFC $M(T)$ curve is then interpreted in terms of a competition between the anisotropy energy of the random local magnetization orientations of the individual clusters, thermal agitation energy and energy of the applied field. For all three specimens, the starting temperature of the bifurcation of ZFC and FC $M(T)$ curves, T_B, is higher than T_{CG}, indicating cluster-glass behavior instead of spin-glass behavior. For the specimen with $x = 1.2$, a cusp presents at $T_{SG} = 16.19$ K in the ZFC magnetization as shown in figure 2(a), which is due to the cluster-glass to spin-glass transition, as indicated by our ac susceptibility measurement shown later. For $Pr_{2-x}Sr_xCoO_4$ with $x = 1.3$ and 1.5, the cusp disappears as shown in figures 2(b) and (c). Another interesting phenomenon is that the FC $M(T)$ curve of the $x = 1.2$ sample shows nonmonotonic behavior when $T < T_{CG}$. In contrast, the FC magnetization for $x = 1.3$ and 1.5 increases monotonically with decreasing temperature when $T < T_{CG}$. The nonmonotonic FC $M(T)$ curve for the $x = 1.2$ sample may indicate a higher percentage of the antiferromagnetic matrix in the material system compared with that of the $x = 1.3$ and 1.5 samples. As shown in figure 2(d), the $\chi^{-1}(T)$ curve of the $x = 1.2$ sample shows downward deviation at $T_G = 201.57$ K, which is characteristic of the formation of a Griffiths phase. For the $x = 1.3$ and 1.5 samples, the $\chi^{-1}(T)$ curves increase linearly with increasing temperature following the Curie–Weiss law above the Curie temperature T_C as shown in figures 2(e) and (f). The magnetic parameters obtained in the experiments are summarized in table 1. With increasing Sr doping, the temperature of the ZFC magnetization peak T_{CG}, the Weiss temperature θ and the Curie temperature T_C increase, confirming the enhancement of the ferromagnetic property, which is also suggested by the monotonically increasing magnetization value with increasing x as shown in figures 2(a)–(c).

To investigate the magnetic glassy behavior of the specimen, we performed ac susceptibility measurements in

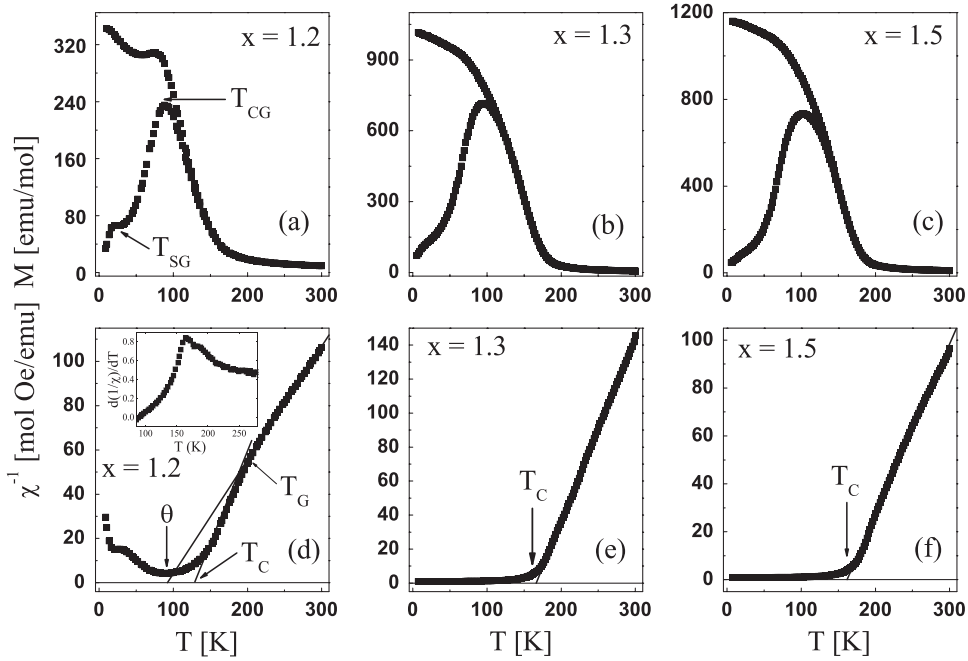

Figure 2. Temperature dependence of the ZFC and FC magnetizations for $x = 1.2$ (a), 1.3 (b) and 1.5 (c) and the inverse susceptibilities $\chi^{-1}(T)$ for $x = 1.2$ (d), 1.3 (e) and 1.5 (f). The inset in (d) is $\mathrm{d}(\chi^{-1})/\mathrm{d}T$ as a function of temperature for $x = 1.2$ and the solid lines in (d), (e) and (f) are the best fit to the Curie–Weiss law in the paramagnetic range.

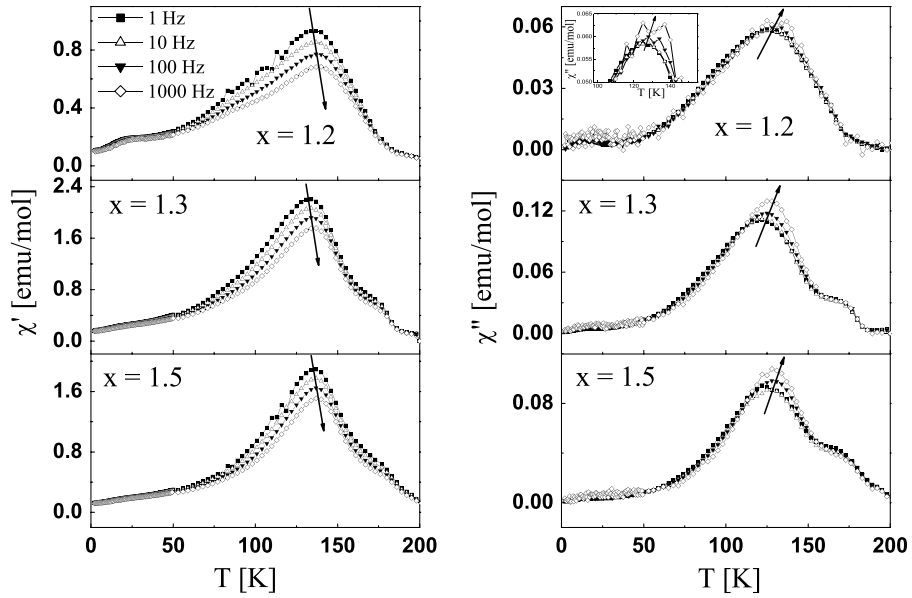

Figure 3. Temperature dependence of the ac susceptibility for $Pr_{2-x}Sr_xCoO_4$, the in-phase $\chi'(T)$ ($x = 1.2$ (a), 1.3 (c) and 1.5 (e)) and out-of-phase $\chi''(T)$ ($x = 1.2$ (b), 1.3 (d) and 1.5 (f)) components in an ac field of 2 Oe at different frequencies, 1, 10, 100 and 1000 Hz. The inset in (b) is the enlarged figure around the peak and the arrows denote the frequency evolution of susceptibility.

a 2 Oe driving field with frequencies of 1, 10, 100 and 1000 Hz. Figure 3 displays the temperature dependence of in-phase $\chi'(T)$ and out-of-phase $\chi''(T)$ components of ac susceptibilities for $Pr_{2-x}Sr_xCoO_4$ at various frequencies. A distinct peak is present in both $\chi'(T)$ and $\chi''(T)$ for all the specimens around T_B. The peaks are frequency-dependent and shift monotonically toward a higher temperature when the frequency of the ac field is increased, as indicated by the arrows in figure 3. The frequency dependence of $T_B(f)$ can be characterized by a p factor:

$$p = \frac{\delta T_B(f)}{T_B(f)\delta \log_{10} f} \sim 6 \times 10^{-4},$$

which is much smaller than the typical values for canonical spin-glass systems in which p ranges from 0.0045 to 0.25 [16, 17]. The result suggests that the magnetic glass

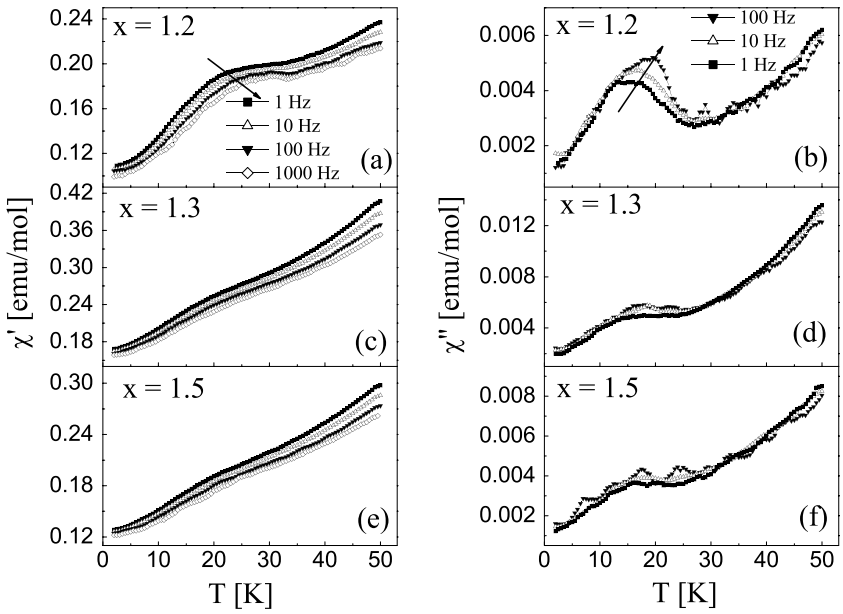

Figure 4. Amplified graph of ac susceptibility versus temperature for $Pr_{2-x}Sr_xCoO_4$ at low temperatures. The arrows in (a) and (b) denote the frequency evolution of susceptibility.

Table 1. Magnetic parameters of $Pr_{2-x}Sr_xCoO_4$: temperature of ZFC magnetization peak T_{CG}, Weiss temperature θ and Curie temperature T_C.

	x		
	1.2	1.3	1.5
T_{CG} (K)	88.05	93.06	100.97
θ (K)	91.89	157.29	161.76
T_C (K)	129.24	157.29	161.76

state in the present specimens belongs to a cluster-glass state. Besides the peak around T_B, the specimens with $x = 1.3$ and 1.5 present a frequency-independent bend near T_C, which is different from other ferromagnetic materials that possess a strong and frequency-independent peak in both $\chi'(T)$ and $\chi''(T)$ at T_C [4, 18]. The specimen with $x = 1.2$ displays a continuous change without any anomaly around T_C. Because the sharpness of the peak in both $\chi'(T)$ and $\chi''(T)$ is a sign of a homogeneous phase transition, the broad bend ($x = 1.3$ and 1.5) and disappearance of the anomaly ($x = 1.2$) may be due to the mixed magnetic phases of the specimens, e.g. ferromagnetic phase and cluster-glass phase.

It is worth noting that another anomaly exists in both $\chi'(T)$ and $\chi''(T)$ for $x = 1.2$ at low temperatures. The 'close-up' figure of the ac susceptibility curve in the low temperature range is shown in figure 4. The $\chi''(T)$ data at $f = 1000$ Hz is too noisy to be compared with other data, therefore we only present the data at low frequencies. For the $x = 1.2$ specimen, a bend in $\chi'(T)$ and a peak in $\chi''(T)$ emerge close to the temperature of the cusp structure in the ZFC magnetization, T_{SG}. Both shift monotonically towards a higher temperature with increasing frequency, indicated by arrows in figures 4(a) and (b). The factor for the frequency dependence of $T_B(f)$, $p \sim 0.049$, is rightly among the typical values for canonical spin-glass systems, suggesting the magnetic glass state is a spin-glass state rather than a cluster-glass state. The bend in $\chi'(T)$ weakens for $x = 1.3$ and disappears for $x = 1.5$ as shown in figures 4(c) and (e). As shown in figures 4 (d) and (f), the $\chi''(T)$ curves of the $x = 1.3$ and 1.5 samples also show one peak. However, in contrast to that of the $x = 1.2$ sample, the position of the peak is frequency-independent, which demonstrates that the spin-glass state vanishes in the specimen with $x = 1.3$ and 1.5.

The existence of a Griffiths phase and spin-glass state for $x = 1.2$ and the disappearance of them in the specimen with increasing doping is also confirmed by the ac susceptibility measurements with an applied magnetic field. Figure 5 presents the in-phase ac susceptibility χ_{ac} measured on warming following zero-field cooling in a driving field amplitude of 2 Oe under a static magnetic field of 1 kOe. For the specimen with $x = 1.2$, a peak and a shoulder are present near the temperature of T_{CG} and T_{SG}, respectively. As indicated by arrows in figure 5(a), they are extremely sensitive to the frequency that move to the higher temperature as frequency increases, demonstrating the dynamic effect of the spin/cluster glass. In the glassy state, magnetic spins experience random interactions with other magnetic spins, resulting in a state that is highly irreversible and metastable. The frequency dependence is a direct indication of the critical dynamics of the spin/cluster-glass system. In figure 5(c) the inverse ac susceptibility for the specimen with $x = 1.2$ also exhibits a downward deviation at 200.7 K that coincides with the temperature of T_G determined from dc magnetism, which is a significant response signal of the Griffiths phase. The ferromagnetic clusters emerge in the paramagnetic matrix, drastically lifting the magnetization value of the system. The abrupt increasing magnetization induces the deviation from Curie–Weiss law for the paramagnetism. However, for the specimen with $x = 1.5$, as shown in figures 5(b) and (d), the

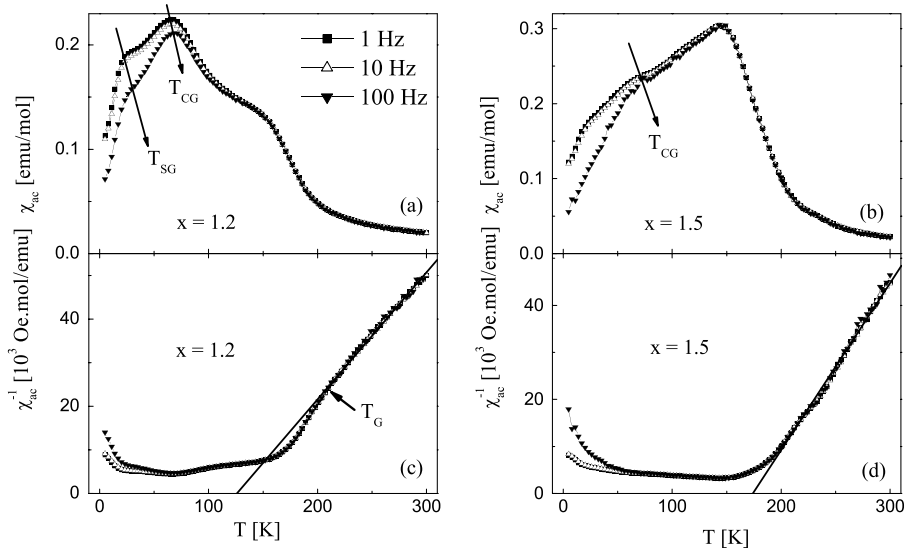

Figure 5. Temperature dependence of the ac susceptibility for $x = 1.2$ (a) and 1.5 (b) and the inverse ac susceptibility for $x = 1.2$ (c) and 1.5 (d) at different frequencies, measured on warming following zero-field cooling in a driving field amplitude of 2 Oe under a static magnetic field of 1 kOe. The arrows in (a) and (b) denote the frequency evolution of susceptibility and the solid lines in (c) and (d) are the best fit to the Curie–Weiss law in the paramagnetic range.

shoulder due to the spin-glass state disappears and the inverse susceptibility above T_C obeys the Curie–Weiss law well.

Figure 6 shows the magnetic hysteresis loops of the $x = 1.2$ sample at various temperatures. At 240 K, a temperature just above T_G, the loop presents a paramagnetic behavior with magnetization increasing linearly with the external magnetic field and without any hysteresis. At 180 K, a temperature between T_G and T_C ($T_C = 129.24$ K, defined from the maximum of $d(\chi^{-1})/dT$ versus temperature), a small hysteresis appears in the loop, indicating a short range ferromagnetic interaction in the specimen, which is the characteristic of a Griffiths singularity due to the coexistence of ferromagnetic entities within the globally paramagnetic phase far above the magnetic ordering temperature [19]. At 120 and 80 K, the sample is in a ferromagnetic state and shows a magnetic loop with clear hysteresis. The coercive field H_C at 80 K is much larger than that at 120 K, just as in a conventional ferromagnet in which H_C continuously increases with decreasing temperature below T_C [4].

Combining the aforementioned experimental results, we can conclude that the $x = 1.2$ sample shows a paramagnetic phase above 201.57 K, a Griffiths phase between 201.57 and 129.24 K, a ferromagnetic cluster-glass phase between 129.24 and 16.19 K and a spin-glass state reentrance below 16.19 K. The downward deviation in the inverse susceptibility ($T_G = 201.57$ K) and cusp structure ($T_{SG} = 16.19$ K) in ZFC magnetization is due to the crossover from paramagnetic state to Griffiths phase and from cluster-glass state to spin-glass state, respectively. To our knowledge, it is the first time to find the coexistence of cluster-glass and spin-glass states in the layered transition-metal oxides, although the coexistence of them has been suggested in perovskite manganese oxides [20]. For $Pr_{2-x}Sr_xCoO_4$ with $x = 1.3$ and 1.5, the linear evolution of dc/ac susceptibilities with temperature and the absence of the cusp in the $M(T)$ curve suggest the disappearance of the

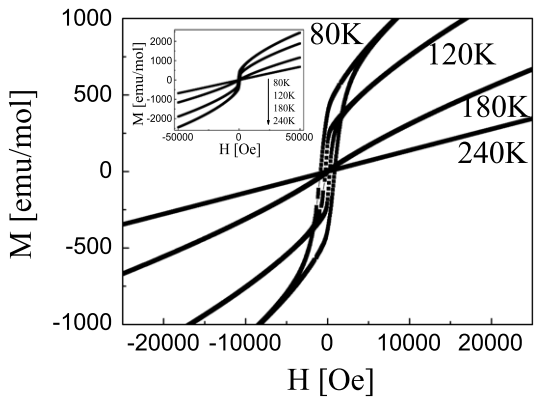

Figure 6. Magnetic hysteresis loops for the $x = 1.2$ sample at 80 K, 120 K, 180 K and 240 K, respectively. Loops are measured by starting at 50 kOe, sweeping to −50 kOe, and then returning to 50 kOe. The inset is the loops in the expanded region out to 50 kOe.

Griffiths phase and spin-glass state, which indicates that the material system changes from a magnetic glassy state to a ferromagnetic state with increasing Sr doping.

Figure 7 shows the magnetic hysteresis loops for $Pr_{2-x}Sr_xCoO_4$ with $x = 1.2$, 1.3 and 1.5 at 10 and 30 K. The loop measured at 10 K shows a larger value of coercive field compared with that measured at 30 K. With increasing doping level, the gradient of the magnetic hysteresis loops becomes steeper around the coercive field. These results are consistent with the enhancement of the ferromagnetic property with increasing Sr doping as aforementioned. It is worth noting that the magnetization of the three samples does not reach saturation in an applied field as high as 5 T at the experimental temperatures. The phenomenon can be clarified through considering the complicated magnetic interactions in the system.

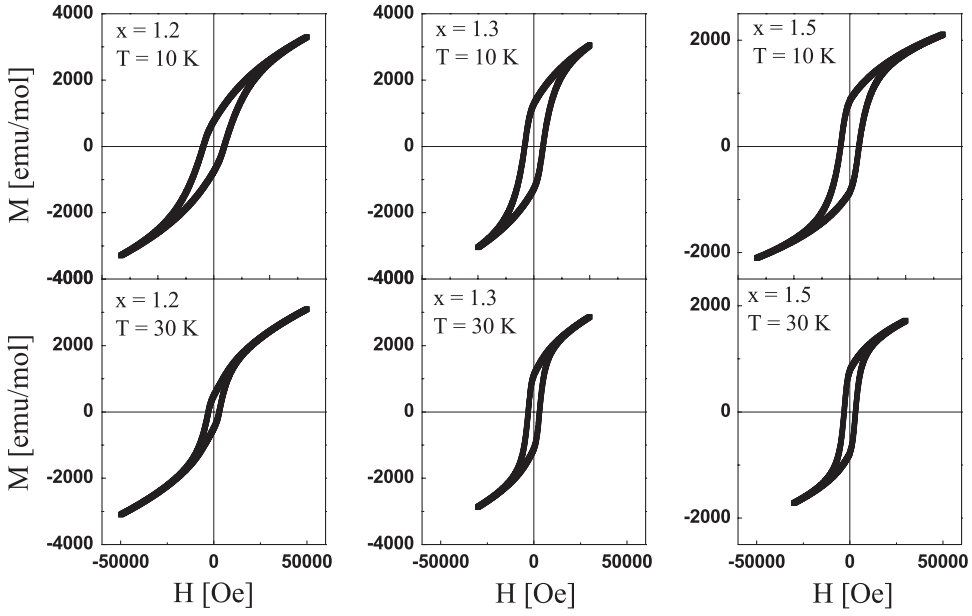

Figure 7. Magnetic hysteresis loops for $Pr_{2-x}Sr_xCoO_4$ ($x = 1.2$, 1.3 and 1.5) at 10 K and 30 K, respectively.

In perovskite cobalt oxides, $Ln_{1-x}Sr_xCoO_3$ (Ln = Nd and Pr) [4, 21–26], there are two kinds of magnetic phases, hole-rich ferromagnetic clusters dominated by the ferromagnetic double exchange between Co^{3+}–Co^{4+} ions and hole-poor antiferromagnetic matrices dominated by antiferromagnetic superexchange interactions between Co^{3+}–Co^{3+} and Co^{4+}–Co^{4+} ions. For the present specimen $Pr_{2-x}Sr_xCoO_4$ in the doping range $x > 1.0$, there are only Co^{3+} and Co^{4+} ions, which have similar magnetic interactions in addition to ferromagnetic interactions between Co^{4+}–Co^{4+} ions as in $SrCoO_3$ [27] and Sr_2CoO_4 [13]. The randomness of the Pr and Sr positions and the complicated magnetic interactions induce a spin/cluster-glass behavior. The replacement of Pr by Sr brings two tremendous effects to the system. First, the antiferromagnetic interactions between Pr^{3+} and Co^{3+} ions are diminished for the decreases of the relevant ions, whereas the ferromagnetic interactions are enhanced for the increasing amount of Co^{4+}. Second, the bigger ionic radius of Sr^{2+} on the A site reduces the Co–O–Co bond length and increases the Co–O–Co bond angle, which leads to a larger tolerance factor for the perovskite structure and a consequent increase in the energy bandwidth of the e_g electrons. In the case of the simple double-exchange ferromagnet, the kinetic energy of the double-exchange carriers scales linearly with the conduction bandwidth [28]. The broadened bandwidth promotes the double exchange of the carriers that enhances the ferromagnetic property. Thus the ferromagnetic order phase emerges and the antiferromagnetic phase diminishes with increasing doping level. However, the antiferromagnetic order phase will not disappear until the ultimate substitution $x = 2.0$ where no Pr^{3+} and Co^{3+} exists in the sample. The coexistence of ferromagnetic cluster and antiferromagnetic matrix results in unsaturated magnetization even in 5 T field.

Figure 8 shows the temperature dependence of resistivity for the $x = 1.2$, 1.3 and 1.5 samples. The specimen

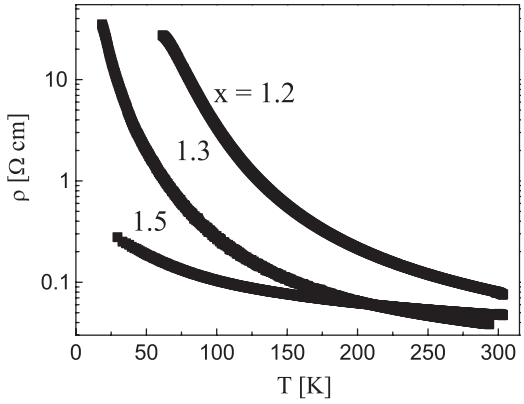

Figure 8. Temperature dependence of the resistivity for $Pr_{2-x}Sr_xCoO_4$ ($x = 1.2$, 1.3 and 1.5).

presents a semiconducting-like behavior ($d\rho/dT < 0$) in the whole temperature range. The semiconducting-like behavior diminishes as x increases. For $x = 1.2$, the relationship between resistivity and temperature follows the Arrhenius law:

$$\rho(T) = \rho_0 \exp\left(\frac{E_\rho}{\kappa_B T}\right),$$

in a wide temperature range as shown in figure 9(a), where ρ_0, E_ρ, k_B and T are the constant determined by material system, the activation energy for conduction, the Boltzmann constant and the absolute temperature. But for $x = 1.3$, only the resistivity at higher temperatures can be fitted with this model as shown in figure 9(b). The $\rho(T)$ at low temperatures as shown in figure 9(c) obeys Mott's two-dimensional variable range hopping (2D VRH) model:

$$\rho(T) = \rho_0 \exp\left[\left(\frac{T_0}{T}\right)^{\frac{1}{3}}\right]$$

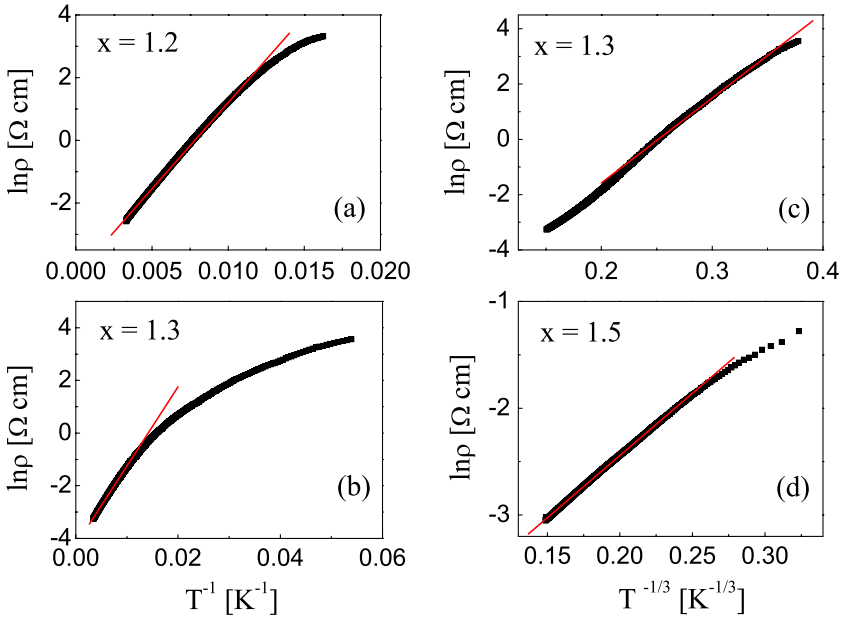

Figure 9. ln ρ versus T^{-1} curves for $x = 1.2$ (a) and $x = 1.3$ (b) and ln ρ versus $T^{-1/3}$ curves for $x = 1.3$ (c) and $x = 1.5$ (d). (This figure is in colour only in the electronic version)

with

$$T_0 \approx \frac{21}{\kappa_B N(E_F)\xi^3},$$

where ξ and $N(E_F)$ are the localization length and the density of localized states at the Fermi energy, respectively [29]. For the $x = 1.5$ sample, the resistivity can be expressed with the 2D VRH model as shown in figure 9(d) except for several points in a narrow low temperature range.

Figure 10 shows the temperature dependence of thermopower S for the $x = 1.2$ and 1.5 samples. The S value for the $x = 1.2$ sample is larger than that for the $x = 1.5$ sample, and both keep positive in the whole temperature range measured, indicating p-type conduction for the specimen. The $S(T)$ curve for both samples decreases monotonically with decreasing temperature and shows a step-like decrease at about 210 K, near the temperature T_G where the linear $\chi^{-1}(T)$ starts to show a downward deviation as shown in figure 2(d). The step-like change for the $x = 1.5$ sample is relatively smaller than that for the $x = 1.2$ sample. As discussed in the literature [30], the step-like decrease is due to the spin alignment from paramagnetic phase to Griffiths phase that increases the charge mobility for the reduction of spin scattering. The temperature for the step-like decrease in the $S(T)$ curve is higher than the T_G in the $\chi^{-1}(T)$ curve, which may be due to their different measuring process. The $S(T)$ curve was measured in the cooling-down process, while the $M(T)$ curve is measured when the system warms up. The appearance of a step-like decrease for the specimen with $x = 1.5$ suggests that the Griffiths phase also exists in the specimen although the $\chi^{-1}(T)$ curve does not show any downward deviation, which may indicate that the thermopower measurement is a more sensitive technique to detect spin-state changes compared with the magnetization measurement.

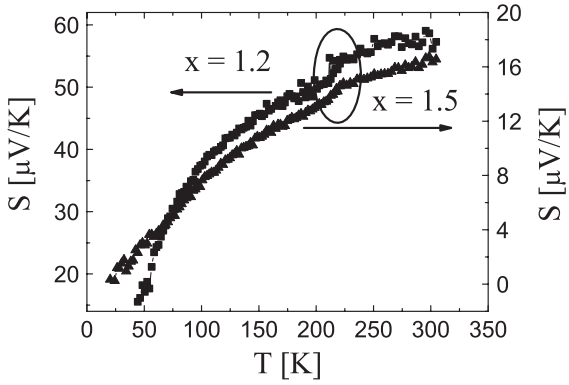

Figure 10. Temperature dependence of the thermopower for $Pr_{2-x}Sr_xCoO_4$ ($x = 1.2$ and 1.5).

The detailed analysis of the temperature dependence of thermopower is shown in figure 11. For the $x = 1.2$ sample, the $S(T)$ curve can be described with thermally activated (intrinsic) conduction:

$$S(T) = \pm\frac{\kappa_B}{e}\left(\frac{E_S}{\kappa_B T} + A\right),$$

where e, E_S and A are the electron charge, the activation energy and the constant related to the effective masses of the electrons and holes, respectively. The linear relationship between $S(T)$ and T^{-1} is shown in figure 11(a). For the $x = 1.5$ sample, the $S(T)$ curve as shown in figure 11(b) can be fitted with 2D VRH conduction:

$$S(T) \propto \frac{\kappa_B}{e}\left(\frac{T_{0S}}{T}\right)^{\frac{1}{3}},$$

where T_{0S} is the characteristic temperature similar to the temperature T_0 in the VRH formula as mentioned

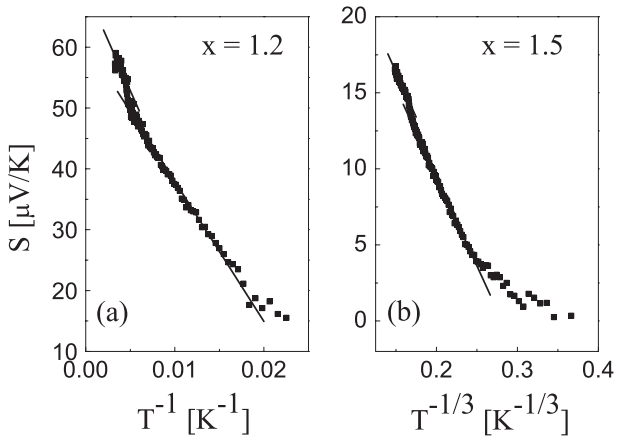

Figure 11. S versus T^{-1} curve for $x = 1.2$ (a) and S versus $T^{-1/3}$ for $x = 1.5$ (b) for $Pr_{2-x}Sr_xCoO_4$.

above [31]. Therefore both the electric transport and the thermal transport measurements indicate that the transport property of $Pr_{2-x}Sr_xCoO_4$ changes from intrinsic conduction to VRH conduction when the Sr doping increases from $x = 1.2$ to 1.5, which may be due to the disorder in the electronic structure caused by the doping. For the specimen with $x = 1.2$, the activation energy obtained from the $\rho(T)$ curve fitting is $E_\rho \approx 47$ meV, while the activation energy obtained from $S(T)$ curve fitting is $E_S \approx 3$ meV. The significant difference between E_ρ and E_S indicates that transport properties of the specimen with $x = 1.2$ may be considered as a small polaron hopping. An electron polarizes the magnetic moment of the ions around it, forming in effect a small ferromagnetic region. The combination of the electron and its strain field is known as a polaron. Magnetic polarons are localized as a consequence of magnetic interactions or at impurities, so that conduction proceeds via thermal hopping [32]. According to the polaron model, the measured activation energy E_ρ is the sum of the activation energy needed for the creation of the carriers and activating the hopping of carriers, and E_S is the energy required to activate the hopping of carriers. Therefore the activation energy E_ρ is larger than E_S. For the intermediate spin-state configurations of the cobalt ions, $t_{2g}^5e_g^1$ for Co^{3+} and $t_{2g}^4e_g^1$ for Co^{4+}, are both susceptible to Jahn–Teller distortions of dynamical and static natures because of the orbital degeneracy of the e_g state. The polaron conduction might result from the strong electron–phonon interactions related to the Jahn–Teller lattice distortion, just as the conduction mechanism of $La_{1-x}Sr_xCoO_3$ [33, 34], $La_{5/8-x}Pr_xCa_{3/8}MnO_3$ [35], $La_{2-x}Sr_xCoO_4$ [36] and $Nd_{2-x}Sr_xCoO_4$ [12].

4. Conclusion

Magnetic, electric transport and thermal transport properties of $Pr_{2-x}Sr_xCoO_4$ with $x = 1.2$, 1.3 and 1.5 have been systematically studied at various temperatures. In dc magnetization the specimen with $x = 1.2$ shows abundant magnetic features in different temperature ranges, including paramagnetic phase above 201.57 K, Griffiths singularity between 201.57 and 129.24 K, ferromagnetic cluster-glass state between 129.24 and 16.19 K, and spin-glass state below 16.19 K. The observation of the rich magnetic phases is also confirmed by magnetic hysteresis loops at different temperatures and ac susceptibilities at different frequencies. With the increasing Sr doping level, the magnetic glassy behavior is suppressed and the transport mechanism of the specimen changes from thermally activated conduction to variable range hopping conduction. The evolution was suggested to be due to the complicated magnetic interactions and Jahn–Teller distortion of the cobalt ions associated with small polarons.

Acknowledgments

The present research is supported by the Singapore A*star SERC grant no. 062 101 0030 and MOE ARC grant no. RG 59/06.

References

[1] Raccah P M and Goodenough J B 1967 *Phys. Rev.* **155** 932
[2] Itoh M, Natori I, Kubota S and Motoya K 1994 *J. Phys. Soc. Japan* **63** 1486
[3] Nam D N H, Jonason K, Nordblad P, Khiem N V and Phuc N X 1999 *Phys. Rev.* B **59** 4189
[4] Wu J and Leighton C 2003 *Phys. Rev.* B **69** 174408
[5] Stauffer D D and Leighton C 2004 *Phys. Rev.* B **70** 214414
[6] Yamada K, Matsuda M, Endo Y, Keimer B, Birgeneau R J, Onodera S, Mizusaki J, Matsuura T and Shirane G 1989 *Phys. Rev.* B **39** 2336
[7] Moritomo Y, Higashi K, Matsuda K and Nakamura A 1997 *Phys. Rev.* B **55** R14725
[8] Helme L M, Boothroyd A T, Prabhakaran D, Wondre F R, Frost C D and Kulda J 2004 *Physica* B **350** e273
[9] Shimada Y, Miyasaka S, Kumai R and Tokura Y 2006 *Phys. Rev.* B **73** 134424
[10] Chichev A V *et al* 2006 *Phys. Rev.* B **74** 134414
[11] Wang X L and Takayama-Muromachi E 2005 *Phys. Rev.* B **72** 064401
[12] Huang S *et al* 2006 *Phys. Rev.* B **73** 094431
[13] Matsuno J, Okimoto Y, Fang Z, Yu X Z, Matsui Y, Nagaosa N, Kawasaki M and Tokura Y 2004 *Phys. Rev. Lett.* **93** 167202
[14] Ang R, Sun Y P, Luo X, Hao C Y and Song W H 2008 *J. Phys. D: Appl. Phys.* **41** 045404
[15] Sanchez-Andujar M and Antonia Senaris-Rodriguez M 2004 *Solid State Sci.* **6** 21
[16] Mydosh J A 1993 *Spin Glasses: an Experimental Introduction* (London: Taylor and Francis)
[17] Satoh T, Kikuchi Y, Miyano K, Pollert E, Hejtmanek J and Jirak Z 2002 *Phys. Rev.* B **65** 125103
[18] Phan T L, Phan M H, Khiem N V, Phuc N X and Yu S C 2004 *J. Magn. Magn. Mater.* **282** 299
[19] Deisenhofer J *et al* 2005 *Phys. Rev. Lett.* **95** 257202
[20] Karmakar S, Taran S, Chaudhuri B K, Sakata H, Sun C P, Huang C L and Yang H D 2006 *Phys. Rev.* B **74** 104407
[21] Yan J-Q, Zhou J-S and Goodenough J B 2004 *Phys. Rev.* B **69** 134409
[22] Fondado A, Breijo M P, Rey-Cabezudo C, Sanchez-Andujar M, Mira J, Rivas J and Senaris-Rodriguez M A 2001 *J. Alloys Compounds* **323/324** 444
[23] Mahendiran R and Schiffer P 2003 *Phys. Rev.* B **68** 024427
[24] Paraskevopoulos M, Hemberger J, Krimmel A and Loidl A 2001 *Phys. Rev.* B **63** 224416

[25] Krimmel A, Reehuis M, Paraskevopoulos M, Hemberger J and Loidl A 2001 *Phys. Rev.* B **64** 224404
[26] Yoshii K and Abe H 2003 *Phys. Rev.* B **67** 094408
[27] Potze R H, Sawatzky G A and Abbate M 1995 *Phys. Rev.* B **51** 11501
[28] Tokura Y and Tomioka Y 1999 *J. Magn. Magn. Mater.* **200** 1
[29] Mott N F and Davis E A 1971 *Electronics Process in Non Crystalline Materials* (Oxford: Clarendon)
[30] Huang S L *et al* 2007 *Phys. Lett.* A **363** 473
[31] Kresin V Z and Little W A 1990 *Organic Superconductivity* (New York: Plenum) pp 101–15
[32] Wang S, Li K, Chen Z and Zhang Y 2000 *Phys. Rev.* B **61** 575
[33] Raccah P M and Goodenough J B 1968 *J. Appl. Phys.* **39** 1209
[34] Heikes R R, Miller R C and Mazelsky R 1964 *Physica* **30** 1600
[35] Kim K H, Uehara M, Hess C, Sharma P A and Cheong S-W 2000 *Phys. Rev. Lett.* **84** 2961
[36] Matsuura T, Tabuchi J, Mizusaki J, Yamuchi S and Fueki K 1988 *J. Phys. Chem. Solids* **49** 1403